

# Local vs non-local correlation effects in interacting quantum spin Hall insulators

L. Crippa,<sup>1,2,\*</sup> A. Amaricci,<sup>3,2,†</sup> S. Adler,<sup>1,4</sup> G. Sangiovanni,<sup>1</sup> and M. Capone<sup>2,3,‡</sup>

<sup>1</sup>*Institut für Theoretische Physik und Astrophysik and Würzburg-Dresden Cluster of Excellence ct.qmat, Universität Würzburg, 97074 Würzburg, Germany*

<sup>2</sup>*Scuola Internazionale Superiore di Studi Avanzati (SISSA), Via Bonomea 265, 34136 Trieste, Italy*

<sup>3</sup>*CNR-IOM DEMOCRITOS, Istituto Officina dei Materiali,*

*Consiglio Nazionale delle Ricerche, Via Bonomea 265, 34136 Trieste, Italy*

<sup>4</sup>*Institute of Solid State Physics, TU Wien, A-1040 Vienna, Austria*

The impact of Coulomb interaction on the electronic properties of a quantum spin-Hall insulator is studied using quantum cluster methods, disentangling local from non-local effects. We identify different regimes, according to the value of the bare mass term, characterized by drastically different self-energy contributions. For small mass, non-local correlations start to be important and eventually dominate over local ones when getting close enough to the zero-mass semi-metallic line. For intermediate and large mass, local correlation effects outweigh non-local corrections, leading to a first-order topological phase transition, in agreement with previous predictions.

The description of solids is based on many-electron wave functions built out of Bloch states, i.e. of delocalized eigensolutions of single electrons in a periodic potential [1]. The resulting electronic energy-momentum dispersion is determined by the quantum mechanical amplitude of electrons hopping from site to site of the lattice. Another important “atomistic” ingredient influencing the bandstructure is the relative energetic alignment of the local levels in the material. Electronic wave functions with strong contribution from atoms whose outer shell is lower in energy form mainly valence bands, while the conduction bands are mostly associated to orbitals of the less electronegative elements. If a clearcut distinction in the above sense exists for a set of bands of an insulator at all momenta in the Brillouin zone, then the bandstructure can be adiabatically connected to some atomic limit and is therefore classified as topologically trivial.

Non-trivial topological effects can, on the contrary, arise when there is a sizeable entanglement between conduction and valence electron wave functions in momentum space. This is the situation in the well-known case of tensile strained HgTe [2, 3]. In this II-VI semiconductor, the 6s level of the Hg is empty and forms to a large extent the conduction band. Yet, due to its large atomic number, Hg is subject to sizeable relativistic corrections, that at the  $\Gamma$  point “pull” some of its 6s character down to the valence eigenvalues [4, 5]. This gap inversion is distinct from any atomic limit and the resulting bandstructure can hence be classified by a non-zero global topological  $\mathbb{Z}_2$ -invariant [6–10]

An electron-electron interaction brings about many-body physics and leads to a breakdown of the independent-particle picture [11–15]. In many cases a bandstructure can still be identified, notwithstanding visible lifetime effects that broaden the single-particle eigenvalues of an amount proportional to the electron-electron

scattering rate. This mechanism is encoded in the electronic self-energy which, in addition to the broadening, describes *i*) a renormalization of the energy positions of the local level and *ii*) a modification of the bare hopping amplitudes.

The first of these two effects, namely the correlation-induced modulation of the local atomic splitting (*i*), can induce a change of the topological invariant, a direct repercussion of the aforementioned connection between band ordering and atomic level energies. This has been analyzed in detail within dynamical mean-field theory (DMFT) [16, 17] and non-local extensions thereof [18–20], as well as with quantum variational approaches [21–25]. Within the so-called Bernevig-Hughes-Zhang-Hubbard (BHZH) [4] model, the trivial-to-nontrivial transition driven by the competition between the bare local splitting  $M$  separating the two orbitals and the Hubbard interaction strength  $U$  has been extensively studied [26–34].

The many-body effects on the electron hopping processes, i.e. *ii*, have been instead investigated much less, so far. Since it is crucial to describe the interplay between *i* and *ii* on an equal footing, in this work we use a cluster extension of DMFT [18–20] to quantify the non-local self-energy renormalizations of the bare hopping amplitudes in the BHZH model, for the case of an average occupation of two electrons per site. Our conclusions, summarized in Sec. IV, are to some extent unexpected, considering the fact that we are focusing on the two-dimensional model: the region of the phase diagram where local many-body corrections of the type *i* dominate is fairly extended, in particular for large local orbital energy splitting  $M$  and large interaction  $U$ . In addition, we unveil the existence of a regime where non-local corrections prevail and small- $\mathbf{q}$  instabilities can be expected. Interestingly, such strongly non-local solutions are found for small values of  $M$ , i.e. deep inside the topologically non-trivial phase. Our results thus point towards the existence of a quantum spin Hall insulator in which an onsite repulsion influences primarily the non-local physics.

The paper is organized as follows: after introducing the

\* [lorenzo.crippa@physik.uni-wuerzburg.de](mailto:lorenzo.crippa@physik.uni-wuerzburg.de)

† [amaricci@sissa.it](mailto:amaricci@sissa.it)

‡ [capone@sissa.it](mailto:capone@sissa.it)

model in Sec. I, we discuss in Sec. II the corresponding self-energy structure obtained within cluster dynamical mean-field theory (CDMFT). In Sec. III A we present results for parameters close to the semimetallic line whereas in Sec. III B we focus on the transition from the trivial band- to the non-trivial quantum spin Hall insulator driven by the mass term at intermediate-sizeable values of the Coulomb repulsion. In Sec. IV we assemble our results in a phase diagram and highlight the relative importance between local and non-local self-energy corrections. Before the conclusions, we elaborate on the comparison between the BHZ model and the Kane-Mele-Hubbard (KMH) one.

## I. MODEL AND METHODS

We consider an interacting BHZ model [4] in two dimensions. Using two-component spinors  $\Psi(\mathbf{k}) = (c_{\mathbf{k}a\sigma}, c_{\mathbf{k}b\sigma})$  where  $c_{\mathbf{k}a\sigma}$  is the annihilation operator for an electron with lattice momentum  $\mathbf{k}$  in orbital  $m = a, b$  with spin  $\sigma = \uparrow, \downarrow$  we can write the single-particle part of the Hamiltonian as

$$\sum_{\mathbf{k}} \Psi_{\mathbf{k}\uparrow}^\dagger H(\mathbf{k}) \Psi_{\mathbf{k}\uparrow} + \sum_{\mathbf{k}} \Psi_{\mathbf{k}\downarrow}^\dagger H^*(-\mathbf{k}) \Psi_{\mathbf{k}\downarrow} \quad (1)$$

where

$$H(\mathbf{k}) = \lambda \sin k_x \tau_x + \lambda \sin k_y \tau_y + [M - 2t(\cos k_x + \cos k_y)] \tau_z \quad (2)$$

is written in terms of Pauli matrices in the orbital subspace  $\vec{\tau}$ . The relation between the  $H(\mathbf{k})$  of the two blocks with opposite spins follows from time-reversal symmetry (TRS). The model describes two orbitals with local energies respectively at  $\pm M$ .  $t$  is a standard nearest-neighbor orbital-diagonal hopping while  $\lambda$  is a nearest-neighbor orbital-off-diagonal spin-orbit coupling (SOC) – See Fig. 1. We fix the total occupation per site to 2 (half-filling), set  $\epsilon \equiv 2t$  as our energy unit and choose  $\lambda = 0.3$ .

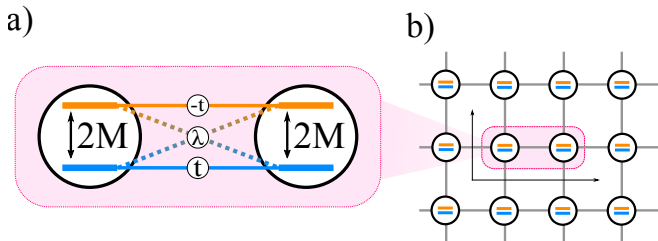


Figure 1. (Color online) (a) Schematic representation of the Hamiltonian of the two-site cluster we use in our CDMFT calculations. (b) Embedding of the cluster in the two-dimensional lattice.

We assume a local interaction within the two-orbital manifold. In particular we use the density-density version of the Slater-Kanamori interaction [35, 36], analo-

gous to previous works on the same model. This interaction depends on a Hubbard repulsion  $U$  and a Hund’s coupling [36, 37]  $J$  describing the interaction between electrons on the same orbital with opposite spins and on different orbitals with same spin, respectively. In our calculations we further consider  $J = U/4$ .

In the absence of interaction, the half-filled model is characterized by a topological phase transition separating a quantum spin-Hall insulator for  $M < 2\epsilon$  and a trivial band insulator for  $M > 2\epsilon$ . Previous analyses have used single-site dynamical mean-field theory (DMFT) [17, 38, 39] to include interaction effects non-perturbatively [27–29, 31–33, 40]. Within DMFT the self-energy is purely local, while retaining the full frequency dependence. The main effect of the interactions is hence a renormalization of the local level splitting, described by the mass term  $M$ . Further, it was previously found that the frequency dependence of the DMFT self-energy influences the thermodynamics of the topological phase transition, which turns from continuous to discontinuous upon increasing the value of the bare Coulomb repulsion  $U$  [40–42].

Here, by means of methods which include short-ranged dynamical correlations [43], namely cluster dynamical mean-field theory [44, 45] (CDMFT) and variational cluster approximation (VCA) [21, 46] we go beyond DMFT and assess the parameters’ region in which the effect of the non-local self-energy corrections are strongest.

## II. CLUSTER-DMFT, THE SELF-ENERGY AND THE TOPOLOGICAL HAMILTONIAN

In CDMFT [44, 45], a real-space extension of DMFT, the lattice model is mapped onto an interacting cluster embedded in a self-consistent bath. Here, we solve the cluster impurity model by means of exact diagonalization [47]. This requires an approximation of the bath in terms of a finite and small number of energy levels [48]. In order to enforce the lattice symmetries, one can organize the bath in a handful of “replicas” of the impurity cluster, each sharing the same symmetry [18, 49, 50]. A schematic representation of the extended impurity problem is presented in Fig. 1. In this work we limit to the smallest two-site cluster and we consider a cluster aligned along the  $x$  direction. This obviously introduces an artificial difference between  $x$  and  $y$ , but it reduces the computational cost, allowing for a reasonable size of the bath (two replicas) and for a systematic investigation of the model parameters.

Within CDMFT we directly obtain the cluster self-energies and Green’s function. Yet, since the CDMFT cluster has open boundary conditions, in order to build lattice observables it is necessary to use a periodization procedure. In this work we employ a  $\Sigma$ -scheme periodization [18, 44] where the lattice self-energy (omitting the

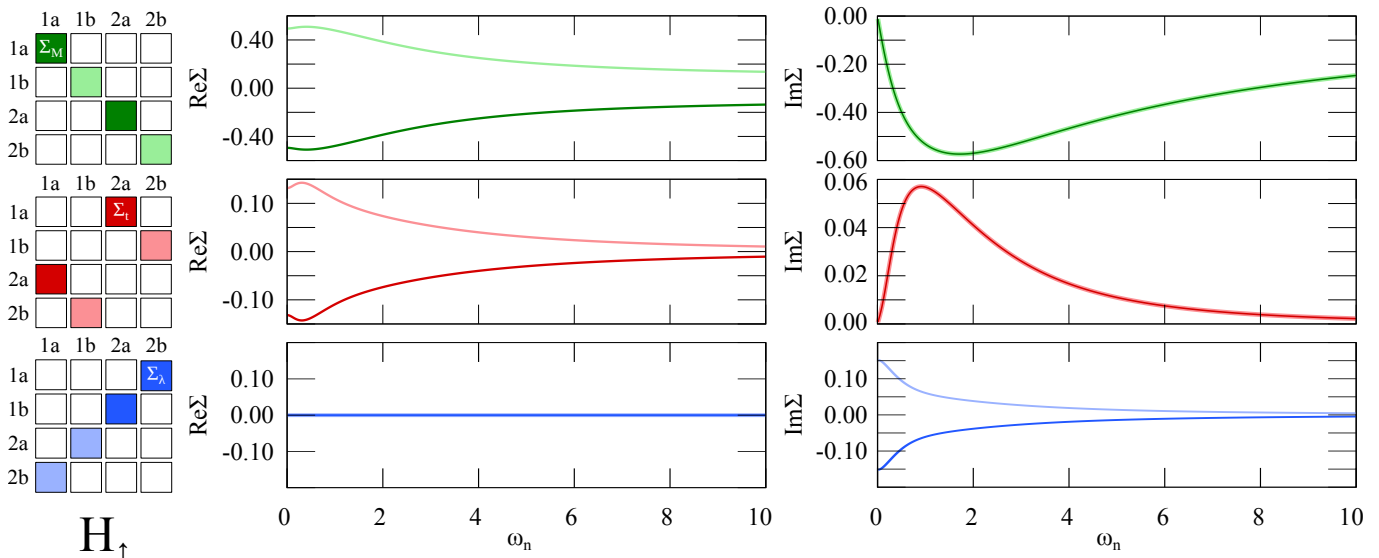


Figure 2. (Color online) Behavior of the cluster self-energy  $\Sigma_{i\alpha\uparrow,j\beta,\uparrow}(i\omega_n)$  on the Matsubara axis for the spin- $\uparrow$  block. The components are indicated in the left column with the colors denoting their symmetries. The cluster sites are labeled by  $i, j = 1, 2$  and the orbitals by roman letters  $\alpha, \beta = a, b$ . The results shown are from CDMFT calculations performed at  $U = 3$  and  $M = 0.8$ , inside the QSHI phase. The spin- $\downarrow$  block's behavior is dictated by symmetries, while all the remaining components vanish within any periodization scheme. Figure adapted from [51].

orbital index) is obtained as

$$\Sigma(\mathbf{k}, z) = \frac{1}{N_C} \sum_{ij} e^{-i\mathbf{k}\cdot(\mathbf{r}_i - \mathbf{r}_j)} [\Sigma]_{ij}(z). \quad (3)$$

with  $[\Sigma]_{ij}$  the self-energy submatrix connecting sites  $i$  and  $j$  of the cluster. This choice of periodization is particularly suited for phases in which the self-energy is regular, as it happens for the topological and trivial insulating states. Other periodizations based on the Green's function and the cumulant [20, 52, 53] are more suited for the study of the Mott insulator and its proximity. We have verified that in the relevant region of parameters that we describe below, the three periodizations yield qualitatively similar results.

The self-energy function  $\Sigma$  in CDMFT has a  $2 \times 2$  (for orbitals) times  $N_C \times N_C$  matrix structure, for each spin. For our  $N_C = 2$  cluster, we have therefore a  $4 \times 4$  matrix with orbital and site indices, as depicted in the left panels of Fig. 2. In these panels we emphasize that the non-zero components of the cluster self-energy mirror the symmetry of the single-particle Hamiltonian and only three independent functions of the frequency are needed to describe the full self-energy. We label these three functions as  $\Sigma_M(i\omega_n)$ ,  $\Sigma_t(i\omega_n)$  and  $\Sigma_\lambda(i\omega_n)$  since they appear as additive corrections to the respective non-interacting parameters. In the  $\Sigma$ -periodization, the three independent functions coincide with the real space components of the cluster self-energy shown in Fig. 2. For example, the middle panels of the figure show  $\text{Re}\Sigma_t(i\omega_n) = \text{Re}\Sigma_{1a,2a} = \text{Re}\Sigma_{2a,1a} = -\text{Re}\Sigma_{1b,2b} = -\text{Re}\Sigma_{2b,1b}$  while the corresponding imaginary parts are identical.

Notice that all imaginary parts other than  $\Sigma_\lambda(i\omega_n)$  vanish in the zero-frequency limit.

We can then express the periodized lattice self-energy in terms of the three independent lattice components introduced above:

$$\Sigma(\mathbf{k}, i\omega_n) = \text{Re}\Sigma_M(i\omega_n)\tau_z + i\text{Im}\Sigma_M(i\omega_n)\tau_0 + [\text{Re}\Sigma_t(i\omega_n)\tau_z + i\text{Im}\Sigma_t(i\omega_n)\tau_0] \cos k_x - \text{Im}\Sigma_\lambda(i\omega_n)\tau_x \sin k_x \quad (4)$$

Comparing with the non-interacting Hamiltonian, we see that  $\Sigma_M(i\omega_n)$ ,  $\Sigma_t(i\omega_n)$  and  $\Sigma_\lambda(i\omega_n)$  play the role of dynamical renormalizations of the three parameters  $M$ ,  $t$  and  $\lambda$  respectively. The form of eq.(4) naturally emerges in the  $\Sigma$  periodization, but it is obtained also with different periodizations as it directly stems from symmetry arguments.

To diagnose the topological properties of interacting systems, various schemes based on effective Hamiltonians as well as on Green's functions [54–56] have been formulated. Here, we make use of the well-established *topological Hamiltonian* [57], defined as

$$H_{\text{topo}}(\mathbf{k}) = H(\mathbf{k}) + \Sigma(\mathbf{k}, \omega = 0). \quad (5)$$

The effect of the interaction on the topological properties is hence described by the zero-frequency limit of  $\Sigma(\mathbf{k}, \omega)$ . Since inversion symmetry is preserved, the construction of the topological index can be further simplified [8, 58], by evaluating the parity of the eigenstates of the occupied bands at the four time-reversal invariant momenta of the square BHZ Brillouin zone.

### III. LOCAL AND NON-LOCAL CORRELATIONS AND THE COMPETITION BETWEEN $M$ AND $U$

The physics of the BHZ model is mostly determined by the interplay and competition between  $U$  and  $M$ . The avoided-crossing for  $M < 2\epsilon$  leading to the band gap is guaranteed by the orbital off-diagonal non-local hybridization  $\lambda$ , whose precise value does not however affect the overall phase diagram. The ratio  $J/U$  determines the critical interaction for the occurrence of the Mott transition but it does not qualitatively influence the properties of the quantum spin Hall phase obtained at intermediate values of  $U$  and  $M$ . The limits of very large  $M$  and  $U$  are expected to host a band- and a Mott insulator, respectively, two topologically trivial phases. For this reason we focus here on the most interesting region where  $U$  and  $M$  are comparable and study the relevance as well as the effect of local and non-local correlations. In particular, we discuss two paradigmatic regions where we find remarkably different correlations effects. These are highlighted in red boxes in the phase diagram that concludes our analysis (Fig. 7): (A) the small  $U$  and small  $M$  parameter range, where a perturbative treatment of the interactions is possible, and (B) the large  $U$  and  $M$  parameter range, where we approach the topological transition and we have fingerprints of Mott-like strong correlations.

#### A. Small-to-intermediate interaction strength

In the spirit of the topological Hamiltonian formulation, in this section and in the following we will study the effect of the interactions through the zero-frequency values of the self-energies, that renormalize the corresponding Hamiltonian parameters. Using the short-cut notation  $\Sigma_l = \Sigma_l(i\omega_n \rightarrow 0)$ , with  $l = M, t, \lambda$ , the eigenvalues of the topological Hamiltonian Eq. (5) reads [59]

$$E_{\pm, \sigma}^2 = [(M + \Sigma_M) - (\epsilon - \Sigma_t) \cos k_x - \epsilon \cos k_y]^2 + (\lambda - \Sigma_\lambda)^2 \sin^2 k_x + \lambda^2 \sin^2 k_y. \quad (6)$$

In all the calculations presented in this work the three self-energies are always negative on the positive Matsubara frequency axis. Hence, from Eq. (6), we find that the effective mass is reduced by the interactions while both non-local terms of the Hamiltonian, i.e. the SOC  $\lambda$  and the orbital-diagonal hopping  $\epsilon$  are increased by the self-energy corrections.

For small values of the interaction the self-energy function can be determined by means of perturbation theory in the interaction  $U$ . This allows to compare the CDMFT results to those obtained within a controlled approximation retaining full momentum dependence. In particular, the contributions to the self-energy components  $\Sigma_l$  can be determined at each order at specific  $k$  points. The first-order term, i.e. the Hartree diagram, influences only  $\Sigma_M$ . The second-order diagrams contributing to the self-energy are depicted in the inset to panel (a) of Fig. 3.

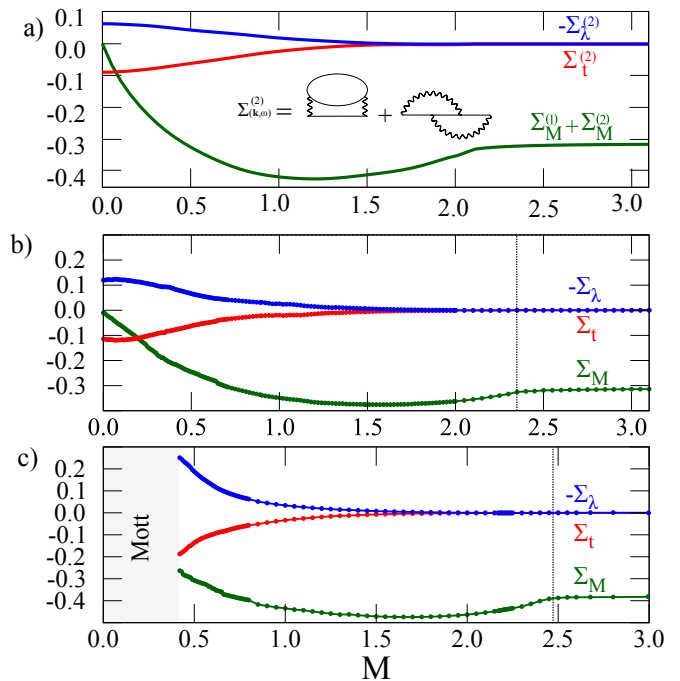


Figure 3. (Color online) The zero-frequency limit of the three relevant components of  $\Sigma$  as a function of  $M$  for two different values of the interaction's strength:  $U = 2.5$  in panels **a)** and **b)** and  $U = 3.5$  in panel **c)**. For  $U = 2.5$ , no Mott transition occurs while, for  $U = 3.5$ , a Mott phase exists at small  $M$  (see also Fig. 7). The topological phase transition driven by  $M$  is indicated by the dotted vertical line. **a)** Self-energy from the lowest order diagrammatic expansion, as sketched by the Feynman diagrams. The system is gapless at the  $[\pi, 0]$  and  $[0, \pi]$  high-symmetry points for  $M = 0$ , and the local component  $\Sigma_M$  vanishes, while  $\Sigma_t$  and  $\Sigma_\lambda$  remain finite. The CDMFT self-energy is shown in **b)** and **c)**. For both values of  $U$ , the main self-energy component at the topological phase transition is  $\Sigma_M$  whereas  $\Sigma_t$  and  $\Sigma_\lambda$  start to dominate upon reducing  $M$ . Figure adapter from [51].

These terms contribute to all the self-energy components in Eq. 6. In panels (a) and (b) of Fig. 3 we compare indeed the perturbative results for an intermediate value of  $U = 2.5$  as a function of  $M$  with the CDMFT results for the same parameters. The perturbative self-energy  $\Sigma^{(2)}(\mathbf{k}, \omega)$  possesses full momentum dependence. Therefore, in order to compare it to the CDMFT results, we assume that Eq. (4), symmetrically extended in the  $k_y$  direction, is a reasonable approximation for the  $k$ -dependent self-energy, and extract the  $\Sigma_{M,t,\lambda}(i\omega)$  coefficients shown in Fig. 3a via a projection onto the corresponding lattice harmonics, i.e. by integrating over the Brillouin zone the quantities  $\Sigma^{(2)}(\mathbf{k}, \omega)$ ,  $\Sigma^{(2)}(\mathbf{k}, \omega) \cos k_x$  and  $\Sigma^{(2)}(\mathbf{k}, \omega) \sin k_x$  respectively.

The agreement is surprisingly good, even at a quantitative level. We can thus infer that a perturbative expansion including local and non-local (momentum-dependent) diagrams is particularly accurate for a relatively large window of interaction. It should be noted

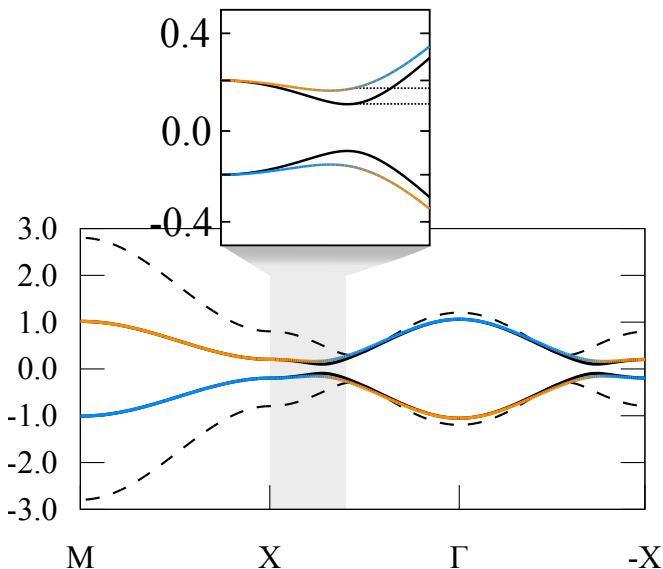


Figure 4. (Color online) Effect of nonlocal correlations as described within CDMFT on the renormalized band structure of the model  $Z_{\mathbf{k}}H(\mathbf{k})$ , in the QSHI region, for  $U = 3$  and  $M = 0.8$ . The path in the Brillouin zone connects the high-symmetry points  $M = [\pi, \pi]$ ,  $\pm X = [\pm\pi, 0]$  and  $\Gamma = [0, 0]$ . The blue and orange bands show the renormalized dispersion in presence of all self-energy contributions, with the projection of the eigenvectors on the two orbitals denoted by the color intensities. The black solid line represents the band dispersion without the orbital off-diagonal component  $\Sigma_{\lambda}$ , while the dashed line is the bare non-interacting dispersion.

that we intentionally do not show a direct comparison deep in the small- $U$  limit, as our numerical implementation with a truncated bath is particularly well suited for intermediate and large interactions and the small values of the self-energies, inevitable for small  $U$ , challenge our numerical accuracy.

The physical picture is non trivial. For  $M = 0$  the non-local self-energies  $\Sigma_t$  and  $\Sigma_{\lambda}$  are finite while the local component  $\Sigma_M$  vanishes [60]. Increasing  $M$  we find a rather rapid decrease of the non-local components, which vanish even before the topological transition is reached. On the other hand the absolute value of  $\Sigma_M$  increases, as found in single-site DMFT, and reaches a maximum where  $\Sigma_t$  and  $\Sigma_{\lambda}$  vanish. For larger values of  $M$ ,  $|\Sigma_M|$  is slightly reduced and stays nearly constant in the trivial band insulator.

If we further increase  $U$  (Fig. 3c) the system is a Mott insulator at small  $M$ . Here, the self-energies diverge. Still, increasing  $M$  we restore a QSH insulator (as already discuss in Refs. [40, 61, 62]). There, the relative qualitative behavior between the various self-energy components discussed for smaller  $U$  is recovered.

As a result, we have a wide region of parameters where the QSHI is affected by local as well as non-local self-energies, beyond the single-site DMFT picture where only  $\Sigma_M$  is nonzero. The bandstructure renormalized by all three CDMFT components,  $\Sigma_t$ ,  $\Sigma_{\lambda}$  and  $\Sigma_M$  is

plotted in Fig. 4. In particular, we show the eigenvalues of  $Z_{\mathbf{k}}H_{\text{topo}}(\mathbf{k})$ , where  $Z_{\mathbf{k}} = [1 - \frac{\partial \Sigma(\mathbf{k}, \omega)}{\partial \omega}|_{\omega=0}]^{-1}$  is the quasiparticle weight measuring the coherence of the low-energy electronic states at different momenta.

The comparison with the non-interacting results shows a non-uniform renormalization in momentum space. A direct effect of the momentum-dependence of the self-energy is visible close to the point where the inverted gap opens (as highlighted in the inset). There we clearly see an increase of the gap, which is easily traced back to the  $\text{Re}\Sigma_{\lambda}$  component enhancing the effective spin-orbit coupling  $\lambda_{\text{eff}} = \lambda - \Sigma_{\lambda}$  according to Eq. 6.

## B. Strong correlation regime

In this section we further increase  $U$  and therefore stabilize the Mott phase. The Mott insulator is rather rigid against the increase of the local orbital splitting, hence we need a sizeable value of  $M$  to stabilize a QSHI (see Fig. 5). The qualitative behavior is quite similar to what we have shown in Fig. 3. The transition from the Mott insulator to the QSHI upon increasing  $M$  is however pushed to such a high value of  $M$  that the small- $M$  region where  $\Sigma_M$  would start to approach zero is completely hidden and we have significant local correlation effects in the whole QSHI phase (in the interval  $2.48 \lesssim M \lesssim 3.06$  for the chosen value of  $U$ ).

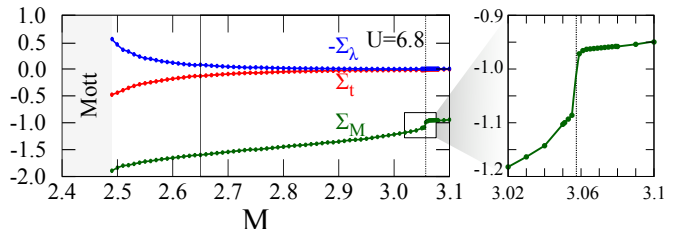


Figure 5. (Color online) The three relevant components of  $\Sigma$  as a function of  $M$  for  $U=6.8$ . The topological phase transition occurs at the vertical dotted line. There, the only relevant self-energy component is  $\Sigma_M$  and its first-order jump highlighted in the right panel.

The CDMFT analysis reveals that, along the topological transition line and pretty irrespectively on  $U$ , the non-local parameters  $t$  and  $\lambda$  are almost unaffected by the interactions. Therefore the gap closing occurs at the  $\Gamma$  point as soon as the first term in (6) becomes zero, i.e. for  $M + \Sigma_M = 2(\epsilon - \frac{\Sigma_t}{2})$ . This expression defines the topological transition line in Fig. 7. Due to the negligible value of  $\Sigma_t$  in this specific range of parameters, we recover the scenario revealed by single-site DMFT [40], where the transition line is given by  $M + \Sigma_M = 2\epsilon$  and it becomes first-order at a critical value of  $U$  and  $M$ .

To further corroborate the evidence of a first-order transition with a non-local approach, we can study the energetic balance of the different solutions. For this, a variational method like variational cluster approximation

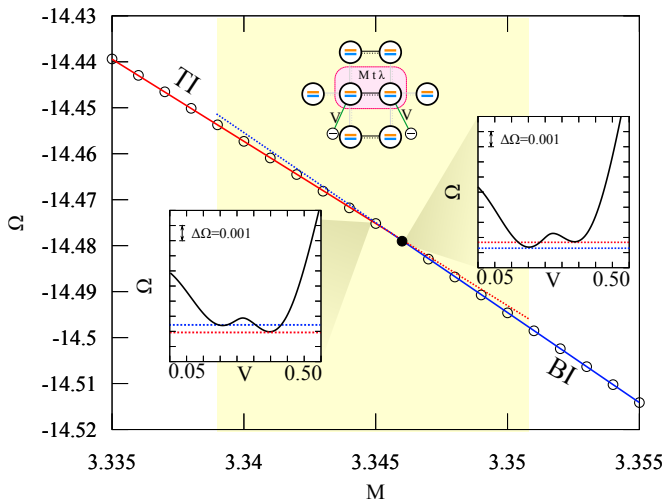


Figure 6. (Color online) Internal energy as a function of  $M$  for  $U = 8$  and across the topological transition. The two lines corresponds to solutions obtained started from the QSHI (red) at small  $M$  or from the BI (blue) at large  $M$ . The filled symbol at the crossing indicates the transition point. Data from VCA calculations. The internal energy is the value of the  $\Omega$  at the stationary point. Insets: The self-energy functional  $\Omega$  as a function of  $V$  for  $M = 3.345$  and  $M = 3.347$ , respectively, before and after the topological transition. The relative position of the minima flips at the transition. Figure adapted from [51].

(VCA) is particularly suited, and in the remaining of this section we present VCA results. Here the solutions are obtained by finding the stationary points of a functional of the cluster self-energy  $\Omega(\Sigma)$  [21, 46, 48]. The value of the functional in the stationary points corresponds to the grand potential of a physical solution with the corresponding self-energy. VCA requires to use a reference system which we choose in analogy with CDMFT as a two site cluster and four additional bath levels (one per orbital and site). The local energy of such effective bath levels is fixed at the chemical potential to enforce the half-filling condition. The hybridization  $V$  among cluster and bath levels is our variational parameter (see the sketch in Fig. 6).

We can therefore follow the evolution of the internal energy of the two solutions (QSHI and BI) as a function of the mass parameter  $M$  (Fig. 6) which clearly shows a wide region of coexistence and a crossing between the two solutions marking the first-order transition. The insets show the behavior of  $\Omega$  as function of the variational parameter  $V$  for two points immediately before and after the TQPT. In both cases the functional shows two minima, separated by a local maximum. In the QSHI phase the minimum is the more strongly hybridized one, whereas the BI solution features a weakly coupled state. As the transition is crossed the global maximum jumps from one of the minima to the other in the same points where the energies cross as a function of  $M$ .

This scenario is completely different from the non-

interacting description of the topological transition, where a single minimum is present for every value of  $M$  and it evolves continuously across the QPT, according to the conventional portrait of topological band theory.

#### IV. LOCAL AND NON-LOCAL CORRELATIONS THROUGH THE PHASE DIAGRAM

We are now in the position to present a global view of the phase diagram in the  $M-U$  plane (Fig. 7) gathering the information encoded in the cuts that we have been discussing so far. The transition line between the QSH and BI phases has a positive slope in the  $U - M$  parameter plane, accounting for the negative sign of the  $\Sigma_M$  component, which opposes the level splitting proportional to  $M$  [40, 61]. A Mott insulating region with uniform orbital occupancy opens for large  $U$ ; as a result, the topologically nontrivial phase intrudes between the trivial Mott ( $U \gg M$ ) and band ( $U \ll M$ ) insulator. We mention that the existence of the high-spin Mott insulator follows from the finite Hund's coupling  $J$  [41].

In the spirit of the present analysis of local and non-local correlations, in the main panel of Fig. 7 we show the ratio between the non-local and local self-energies  $\Sigma_t/\Sigma_M$  in a greyscale. The plot clearly highlights one of the main results emerging from our analysis, namely that the non-local component is comparable with the local one only in a window of small  $M$  and in any case before the Mott transition is reached. In this region we can expect that longer-range correlations become more and more important. Therefore, in contrast with the large- $M$  scenario, where the self-energy is essentially local, larger clusters would be necessary to accurately describe the system.

The rest of the phase diagram is clearly white – signaling that local correlations overwhelm non-local ones – in particular close to the transition line between QSHI and BI. This analysis can not be applied in the Mott insulating phase, where all the self-energy components tend to diverge [18]. This is the origin of the very thin grey border at the boundary of the Mott insulating which is in turn identified with a dashed motif.

The phase diagram shows again that the two regions we have highlighted in the previous sections present a very different competition between local and non-local correlations. In order to highlight this point we show the three components of the self-energy in color scales. The three panels at the bottom of Fig. 7 illustrate the picture at small  $M$ . Here we see that the three components evolve differently. While the local  $\Sigma_M$  increases when both  $U$  and  $M$  are simultaneously increased (it is larger in the top-right corner), the non-local components, and in particular  $\Sigma_t$ , increase with  $U$  and they have a weaker dependence on  $M$  (they are large moving towards the right of the panels). The balance and the competition between the different components is hence rich and sub-

tle. This can be another indication that this region can be strongly affected by including further non-local effects.

On the other hand, the large  $M$  and large  $U$  case (panels on top of Fig. 7) presents a much simpler picture. The local self-energy is large in the whole QSHI phase, while the two local components are basically negligible except for a thin parameter range close to the Mott transition line. In particular, the behavior around the topological transition is dominated by  $\Sigma_M$  and it can be understood within single-site DMFT.

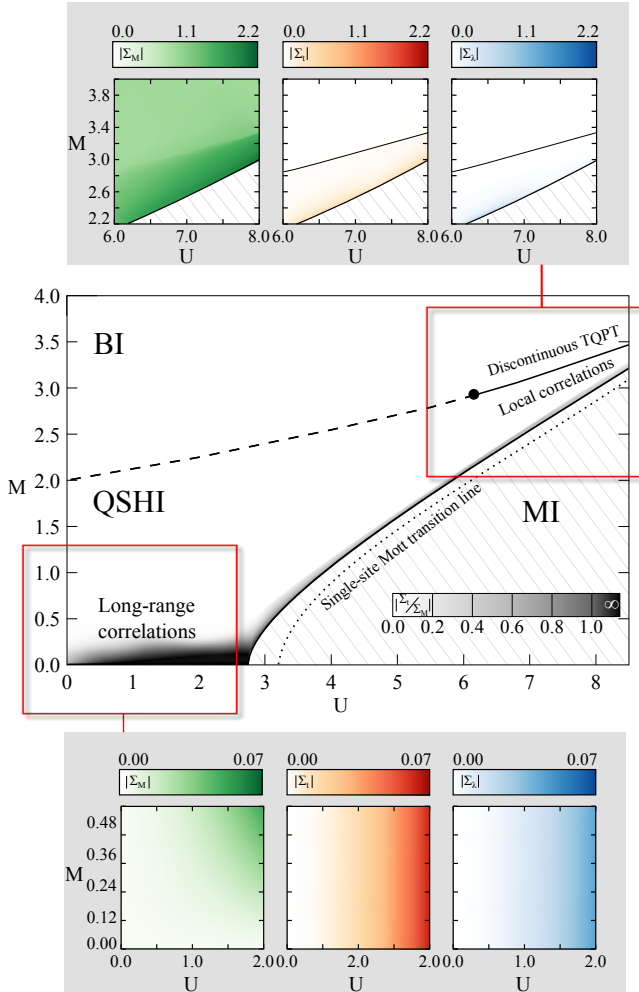


Figure 7. (Color online) CDMFT phase diagram of the half-filled BHZH model in the  $U$ - $M$  plane. The three areas refers to band-, quantum spin Hall- and Mott-insulator (BI, QSHI and MI, respectively). In the upper and bottom gradient insets we show the absolute value of the relative  $\Sigma$  component at zero frequency. The black gradient in the main panel encodes the relative strength of the momentum-dependent component  $\Sigma_t$  with respect to  $\Sigma_M$ . The latter represents the dominant type of correlation in the BI and QSHI regions, except close to the Mott line, in particular in the bottom-left corner at small values of  $M$ . There, even well before the MI phase sets in, the system develops non-local correlations, suggesting the presence of long-range self-energy components.

The characterization of the relative importance of local

and non-local correlation effects on the topological quantum phase transition in the BHZH model naturally calls for a comparison with the KMH model. In the latter, the relevant degrees of freedom for the QSHI state are represented by the non-local sub-lattice flavor, rather than by the local orbitals. The KMH model has been extensively investigated using different methods, e.g. VCA, Hartree-Fock, single-site as well as cluster DMFT [34, 63–67]. The local splitting  $M$  between the two orbitals in the BHZH model is replaced, in the KMH, by the staggered potential between two sublattices of the honeycomb, i.e. the Semenoff mass [34] (see Fig. 8a). Similarly to the BHZH model, this term drives the KMH model towards a trivial phase, reached when  $M$  becomes larger than a critical value  $M_c$  [68]. To the best of our knowledge, there is no evidence of a discontinuous topological transition in this model in the presence of large interactions, in contrast with the results of the BHZH model, raising a question about the role of locality of the interactions as well as of the approximations.

Interestingly, in the closely related (spinful) Haldane model it has been shown by means of a two-particle self-consistent approximation, that close to the topological transition driven by the Semenoff mass at fixed  $U$ , the dominant renormalization is represented by the on-site components of the self-energy [66], similarly to what we found here for the BHZH model. The combination of these results and those here reported, showing that the discontinuous transition of the BHZH model survives the inclusion of non-local effects, suggests that the absence of first-order topological transition in the KMH model is not a consequence of the approximation, but it results from the difference between the two many-body Hamiltonians.

A closer inspection identifies a natural candidate in the interaction terms, which in the BHZH model involves the orbital subspace and in the KMH, the sub-lattice one. Indeed, the BHZH features both a (local) intra-orbital repulsion and a (local) inter-orbital one whereas the KMH – at least in its standard form – has no inter-site term. This breaks the correspondence at the level of the two-body interaction. Indeed, single-site DMFT calculations for the KMH model reported in Appendix A confirm the absence of a discontinuous transition and, most importantly, they share the same qualitative behavior of calculations for the BHZH model in which we artificially switched off the inter-orbital repulsion [40, 41, 61].

Following this analogy we can surmise that the inclusion of non-local components of the electron-electron interaction would provide a route to observe first-order effects in the KMH. Treating the KMH within CDMFT and adding an inter-sublattice interaction mimicking the effect of the Hund’s coupling could potentially give information on the small- $M$  non-local physics as well as on the first-order topological phase transition, which instead in the BHZH model is present already at the single-site DMFT level.

## V. CONCLUSION

We have investigated the electronic correlations throughout the phase diagram of the BHZH model which integrates a typical setup for topological phase transitions and a Hubbard-like local interaction term. We use CDMFT, a quantum cluster extension of DMFT that accurately treats short-ranged correlations inside the cluster. These are interpreted in terms of additive renormalizations of three control model parameters. In particular we have a local term, which renormalizes the mass  $M$  ruling the topological phase transition and two non-local terms correcting the nearest-neighbor hopping  $t$  and the spin-orbit coupling  $\lambda$ , respectively.

This way, we can show how the relative importance of local and non-local correlations changes in a spectacular way according to the bare parameters and, more precisely, that the value of  $M$  has a strong impact. The non-local terms turn out to be comparable with the non-local ones for small  $M$ , as long as the Hubbard  $U$  is not sufficient to drive a Mott transition. On the other hand, local correlation effects are predominant at intermediate and large  $M$  including the whole region around the topological phase transition. This allows us to confirm the robustness of the scenario derived with single-site DMFT, where the topological transition becomes of first-order for intermediate values of  $U$  and  $M$ .

The present results are for phases with no long-range order. It is well known that both BHZH and KMH models host lower symmetry magnetic or charge ordered phases, in particular in the correlated context. Our findings give indications on the nature of the symmetry-broken phases that may develop in the different parameter ranges. At large  $U$  and  $M$ , where local self-energy corrections are found to dominate, we expect instabilities associated to the ordering of local spin- or orbital-moments. The importance of  $\mathbf{k}$ -dependent self-energy corrections at small  $M$  suggests instead the possibility of a wider palette of competing phases. A pronounced itinerant character or the ordering at small momenta may indeed arise close to the orbital-degenerate line  $M = 0$ , where the underlying paramagnetic Mott phase at large  $U$  is driven primarily by non-local components of  $\Sigma$ , rather than by the local ones as in the conventional case.

## VI. ACKNOWLEDGEMENTS

L.C., A.A. and M.C. acknowledge financial support from MIUR through PRIN 2015 (Prot. 2015C5SEJJ001) and PRIN2017 project CEnTral (Protocol Number 20172H2SC4). A.A. and M.C. acknowledge support from H2020 Framework Programme, under ERC Advanced Grant No. 692670 ‘‘FIRSTORM’’. G.S., S.A. and L.C. acknowledge financial support by the Deutsche Forschungsgemeinschaft (DFG, German Research Foundation) under Germany’s Excellence Strategy through Würzburg-Dresden Cluster of Excellence on Complex-

ity and Topology in Quantum Matter - ct.qmat (EXC 2147, project-id 390858490). The authors gratefully acknowledge the Gauss Centre for Supercomputing e.V. (www.gauss-centre.eu) for funding this project by providing computing time on the GCS Supercomputer SuperMUC at Leibniz Supercomputing Centre (www.lrz.de).

## APPENDIX A

The Kane-Mele model is historically the first proposal of a topological insulator presenting a nontrivial quantum spin-Hall effect [68]. The setup consists of two copies of the Haldane model on the honeycomb lattice [69], one for each spin orientation, related by time-reversal symmetry. A Haldane mass term with opposite sign for the two spins is then added: this term, which couples momentum with spin degrees of freedom, arises from spin-orbit coupling. It is also non-local, taking the form of a second-nearest-neighbour hopping amplitude. In contrast with the Haldane model, the Kane-Mele mass term does not break the time-reversal symmetry of the system.

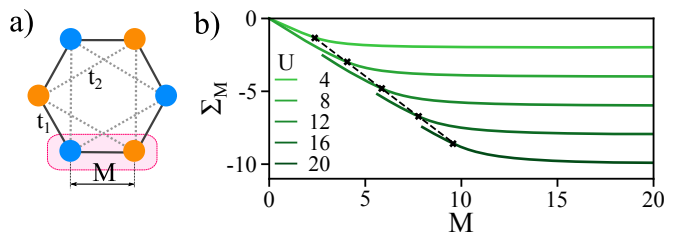


Figure 8. (Color online) **a)** Schematics of the Kane-Mele model on the honeycomb lattice. **b)** Single-site DMFT data for site-diagonal self-energy component  $\Sigma_M$  in the KMH as a function of  $M$  for different values of  $U$ . Every line is continuous independently on how large  $U$  is chosen, denoting the absence of the first-order phase transition. This is at odds with the BHZ model at large  $M$  and large  $U$  where both single-site and cluster DMFT show a jump in  $\Sigma_M$  (see Fig. 5). The black crosses show the location of the topological phase transition in the KMH model.

In reciprocal space, the Hamiltonian matrix of the model has the form

$$H(\mathbf{k}) = \sum_{a=1}^5 d_a(\mathbf{k})\Gamma^a + \sum_{a<b=1}^5 d_{ab}(\mathbf{k})\Gamma^{ab}, \quad (7)$$

where the  $d$  terms are trigonometric functions of the momentum components, and the  $\Gamma$  matrices span the 16 generators of the  $SU(4)$  matrix group (excluding the identity) [70]: in particular, the five  $\Gamma^a$  are the so-called Dirac matrices satisfying the Clifford algebra

$$[\Gamma^\mu, \Gamma^\nu]_+ = 2\delta_{\mu\nu}\mathbb{1}_{4\times 4}$$



while the remaining  $\Gamma^{ab}$  are obtained from the commutators of the Dirac matrices,

$$\Gamma^{\mu\nu} = \frac{1}{2i}[\Gamma^\mu, \Gamma^\nu].$$

The effect of the single-site DMFT self-energy on the topology of the KMH model can be evinced from Fig. 8. As established in the previous sections, the discontinuity in the topological phase transition of the BHZ model is due to the local correlation effects, i.e. to the real part of the local self-energy component  $\Sigma_M$ . Its behavior in the single-orbital KMH model is shown, for various values of the Hubbard interaction, in panel (b), with the topological phase transition points for the different  $M$  values being marked by the black crosses.

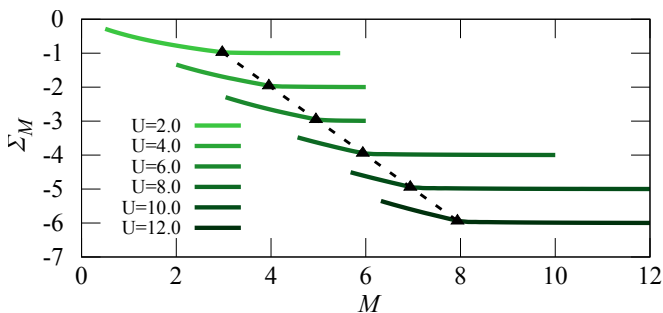


Figure 9. (Color online) Real part of the self-energy for the BHZ model where the interaction term contains no inter-orbital component. The data refer to single-site DMFT, where only the diagonal component is present. The black marks and dotted line refer to the values of  $\Sigma_M$  where the TQPT occurs, the latter being always continuous. As in Fig. 8, and in contrast to Fig. 5, the topological phase transition is always continuous, since  $\Sigma_M$  features no discontinuities.

The comparison of Fig. 8(b) on the one side and Fig. 3 and Fig. 5 on the other evidences two main differences: *i*) the minimum of  $\Sigma_M$  at intermediate values of  $M$  reported in Fig. 3(a) and (b) - which, crucially, characterizes both DMFT and CDMFT results - is absent for the KMH case, and *ii*) the jump at large values of  $U$ , visible in Fig. 5, is not present. Both points can be linked to the difference in the internal structure of the two-body interaction Hamiltonian. This can be shown by comparing these results with a BHZH setup in which  $H_{\text{int}}$  consists of the orbital-diagonal Hubbard  $U$  term only, disregarding all effects of Hund's coupling. This setup is shown in Fig. 9, where the values of  $\Sigma_M$  are again plotted as a function of the bare mass for various interaction strengths. The absence of discontinuities in the self-energy evolution, which reflects in a continuous topological phase transition in the  $U - M$  phase diagram, suggests that the orbital off-diagonal terms of the Slater-Kanamori interaction are the main drivers of the discontinuous TQPT.

- 
- [1] F. Bloch, Über die quantenmechanik der elektronen in kristallgittern, *Zeitschrift für Physik* **52**, 555 (1929).
  - [2] X. Dai, T. L. Hughes, X.-L. Qi, Z. Fang, and S.-C. Zhang, Helical edge and surface states in hgte quantum wells and bulk insulators, *Phys. Rev. B* **77**, 125319 (2008).
  - [3] C. Brüne, C. X. Liu, E. G. Novik, E. M. Hankiewicz, H. Buhmann, Y. L. Chen, X. L. Qi, Z. X. Shen, S. C. Zhang, and L. W. Molenkamp, Quantum hall effect from the topological surface states of strained bulk hgte, *Phys. Rev. Lett.* **106**, 126803 (2011).
  - [4] B. A. Bernevig, T. L. Hughes, and S.-C. Zhang, Quantum spin hall effect and topological phase transition in hgte quantum wells, *Science* **314**, 1757 (2006).
  - [5] D. G. Rothe, R. W. Reinthaler, C.-X. Liu, L. W. Molenkamp, S.-C. Zhang, and E. M. Hankiewicz, Fingerprint of different spin-orbit terms for spin transport in HgTe quantum wells, *New Journal of Physics* **12**, 065012 (2010).
  - [6] C. L. Kane and E. J. Mele, Quantum Spin Hall Effect in Graphene, *Phys. Rev. Lett.* **95**, 226801 (2005).
  - [7] C. L. Kane and E. J. Mele,  $Z_2$  Topological Order and the Quantum Spin Hall Effect, *Phys. Rev. Lett.* **95**, 146802 (2005).
  - [8] L. Fu and C. L. Kane, Topological insulators with inversion symmetry, *Phys. Rev. B* **76**, 045302 (2007).
  - [9] C. L. Kane, Condensed matter: An insulator with a twist, *Nat Phys* **4**, 348 (2008).
  - [10] M. Z. Hasan and C. L. Kane, Colloquium: Topological insulators, *Rev. Mod. Phys.* **82**, 3045 (2010).
  - [11] A. A. Abrikosov and I. M. Khalatnikov, The theory of a fermi liquid (the properties of liquid  $^3\text{He}$  at low temperatures), *Reports on Progress in Physics* **22**, 329 (1959).
  - [12] J. Hubbard and B. H. Flowers, Electron correlations in narrow energy bands, *Proceedings of the Royal Society of London. Series A. Mathematical and Physical Sciences* **276**, 238 (1963).
  - [13] J. Hubbard and B. H. Flowers, Electron correlations in narrow energy bands. ii. the degenerate band case, *Proceedings of the Royal Society of London. Series A. Mathematical and Physical Sciences* **277**, 237 (1964).

- [14] J. Hubbard and B. H. Flowers, Electron correlations in narrow energy bands iii. an improved solution, *Proceedings of the Royal Society of London. Series A. Mathematical and Physical Sciences* **281**, 401 (1964).
- [15] N. F. Mott, The basis of the electron theory of metals, with special reference to the transition metals, *Proceedings of the Physical Society. Section A* **62**, 416 (1949).
- [16] G. Kotliar and D. Vollhardt, Strongly correlated materials: Insights from dynamical mean-field theory, *Physics Today* **57**, 53 (2004).
- [17] A. Georges, G. Kotliar, W. Krauth, and M. J. Rozenberg, Dynamical mean-field theory of strongly correlated fermion systems and the limit of infinite dimensions, *Rev. Mod. Phys.* **68**, 13 (1996).
- [18] M. Capone, M. Civelli, S. S. Kancharla, C. Castellani, and G. Kotliar, Cluster-dynamical mean-field theory of the density-driven mott transition in the one-dimensional hubbard model, *Phys. Rev. B* **69**, 195105 (2004).
- [19] H. Park, K. Haule, and G. Kotliar, Cluster dynamical mean field theory of the mott transition, *Phys. Rev. Lett.* **101**, 186403 (2008).
- [20] S. Sakai, G. Sangiovanni, M. Civelli, Y. Motome, K. Held, and M. Imada, Cluster-size dependence in cellular dynamical mean-field theory, *Phys. Rev. B* **85**, 035102 (2012).
- [21] M. Potthoff, M. Aichhorn, and C. Dahnken, Variational cluster approach to correlated electron systems in low dimensions, *Phys. Rev. Lett.* **91**, 206402 (2003).
- [22] M. Aichhorn, E. Arrighoni, M. Potthoff, and W. Hanke, Variational cluster approach to the hubbard model: Phase-separation tendency and finite-size effects, *Phys. Rev. B* **74**, 235117 (2006).
- [23] D. Sénéchal, The variational cluster approximation for hubbard models: Practical implementation, in *2008 22nd International Symposium on High Performance Computing Systems and Applications* (2008) pp. 9–15.
- [24] M. Balzer, B. Kyung, D. Sénéchal, A.-M. S. Tremblay, and M. Potthoff, First-order mott transition at zero temperature in two dimensions: Variational plaquette study, *EPL (Europhysics Letters)* **85**, 17002 (2009).
- [25] K. Seki, T. Shirakawa, and S. Yunoki, Variational cluster approach to thermodynamic properties of interacting fermions at finite temperatures: A case study of the two-dimensional single-band hubbard model at half filling, *Phys. Rev. B* **98**, 205114 (2018).
- [26] M. Hohenadler and F. F. Assaad, Correlation effects in two-dimensional topological insulators, *Reports on Progress in Physics* **25**, 143201 (2013).
- [27] S. Miyakoshi and Y. Ohta, Antiferromagnetic topological insulator state in the correlated bernevig-hughes-zhang model, *Phys. Rev. B* **87**, 195133 (2013).
- [28] L. Wang, X. Dai, and X. C. Xie, Interaction-induced topological phase transition in the Bernevig-Hughes-Zhang model, *EPL (Europhysics Letters)* **98**, 57001 (2012).
- [29] T. Yoshida, S. Fujimoto, and N. Kawakami, Correlation effects on a topological insulator at finite temperatures, *Phys. Rev. B* **85**, 125113 (2012).
- [30] M. Hohenadler, T. C. Lang, and F. F. Assaad, Correlation effects in quantum spin-hall insulators: A quantum monte carlo study, *Phys. Rev. Lett.* **106**, 100403 (2011).
- [31] A. Amaricci, L. Privitera, F. Petocchi, M. Capone, G. Sangiovanni, and B. Trauzettel, Edge state reconstruction from strong correlations in quantum spin hall insulators, *Phys. Rev. B* **95**, 205120 (2017).
- [32] J. C. Budich, R. Thomale, G. Li, M. Laubach, and S.-C. Zhang, Fluctuation-induced topological quantum phase transitions in quantum spin-Hall and anomalous-Hall insulators, *Phys. Rev. B* **86**, 201407 (2012).
- [33] A. Amaricci, A. Valli, G. Sangiovanni, B. Trauzettel, and M. Capone, Coexistence of metallic edge states and antiferromagnetic ordering in correlated topological insulators, *Phys. Rev. B* **98**, 045133 (2018).
- [34] S. Rachel, Interacting topological insulators: a review, *Reports on Progress in Physics* **81**, 116501 (2018).
- [35] J. Kanamori, Electron Correlation and Ferromagnetism of Transition Metals, *Progress of Theoretical Physics* **30**, 275 (1963).
- [36] A. Georges, L. de' Medici, and J. Mravlje, Strong Correlations from Hund's Coupling., *Annu. Rev. Condens. Matter Phys.* **45**, 137 (2013).
- [37] L. de' Medici, Hund's coupling and its key role in tuning multiorbital correlations, *Phys. Rev. B* **83**, 205112 (2011).
- [38] W. Metzner and D. Vollhardt, Correlated Lattice Fermions in  $d = \infty$  Dimensions, *Phys. Rev. Lett.* **62**, 324 (1989).
- [39] E. Müller-Hartmann, Correlated fermions on a lattice in high dimensions, *Zeitschrift für Physik B Condensed Matter* **74**, 507 (1989).
- [40] A. Amaricci, J. C. Budich, M. Capone, B. Trauzettel, and G. Sangiovanni, First-Order Character and Observable Signatures of Topological Quantum Phase Transitions, *Phys. Rev. Lett.* **114**, 185701 (2015).
- [41] A. Amaricci, J. C. Budich, M. Capone, B. Trauzettel, and G. Sangiovanni, Strong correlation effects on topological quantum phase transitions in three dimensions, *Phys. Rev. B* **93**, 235112 (2016).
- [42] L. Crippa, A. Amaricci, N. Wagner, G. Sangiovanni, J. C. Budich, and M. Capone, Nonlocal annihilation of weyl fermions in correlated systems, *Phys. Rev. Research* **2**, 012023 (2020).
- [43] T. Maier, M. Jarrell, T. Pruschke, and M. H. Hettler, Quantum cluster theories, *Rev. Mod. Phys.* **77**, 1027 (2005).
- [44] G. Kotliar, S. Y. Savrasov, G. Pálsson, and G. Biroli, Cellular dynamical mean field approach to strongly correlated systems, *Phys. Rev. Lett.* **87**, 186401 (2001).
- [45] G. Biroli and G. Kotliar, Cluster methods for strongly correlated electron systems, *Phys. Rev. B* **65**, 155112 (2002).
- [46] M. Potthoff, Self-energy-functional approach to systems of correlated electrons, *The European Physical Journal B - Condensed Matter and Complex Systems* **32**, 429 (2003).
- [47] A. Amaricci, L. Crippa, A. Scazzola, F. Petocchi, G. Mazza, L. de Medici, and M. Capone, Edipack: A parallel exact diagonalization package for quantum impurity problems (2021), [arXiv:2105.06806 \[physics.comp-ph\]](https://arxiv.org/abs/2105.06806).
- [48] D. Sénéchal, Bath optimization in the cellular dynamical mean-field theory, *Phys. Rev. B* **81**, 235125 (2010).
- [49] M. Civelli, *Investigation of strongly correlated electron systems with cellular dynamical mean field theory*, *Ph.D. thesis*, Rutgers The State University of New Jersey - New Brunswick (2006).
- [50] E. Koch, G. Sangiovanni, and O. Gunnarsson, Sum rules and bath parametrization for quantum cluster theories, *Phys. Rev. B* **78**, 115102 (2008).

- [51] L. Crippa, *Local and non-local correlations in Topological Insulators and Weyl Semimetals*, Ph.D. thesis, SISSA (2020).
- [52] D. Sénéchal, D. Perez, and M. Pioro-Ladrière, Spectral weight of the hubbard model through cluster perturbation theory, *Phys. Rev. Lett.* **84**, 522 (2000).
- [53] T. D. Stanescu and G. Kotliar, Fermi arcs and hidden zeros of the green function in the pseudogap state, *Phys. Rev. B* **74**, 125110 (2006).
- [54] J.-H. Zheng and W. Hofstetter, Topological invariant for two-dimensional open systems, *Phys. Rev. B* **97**, 195434 (2018).
- [55] A. A. Markov, G. Rohringer, and A. N. Rubtsov, Robustness of the topological quantization of the hall conductivity for correlated lattice electrons at finite temperatures, *Phys. Rev. B* **100**, 115102 (2019).
- [56] P. Thunström and K. Held, Topology of  $\text{smb}_6$  determined by dynamical mean field theory (2019), [arXiv:1907.03899 \[cond-mat.str-el\]](https://arxiv.org/abs/1907.03899).
- [57] Z. Wang and S.-C. Zhang, Simplified topological invariants for interacting insulators, *Phys. Rev. X* **2**, 031008 (2012).
- [58] Z. Wang, X.-L. Qi, and S.-C. Zhang, Topological invariants for interacting topological insulators with inversion symmetry, *Phys. Rev. B* **85**, 165126 (2012).
- [59] The expression is manifestly non-symmetric due to the choice of the cluster which is aligned along the  $x$  direction, hence non-local self-energies enter only in the  $k_x$  direction. For a more symmetric cluster, the  $k_x$  and  $k_y$  direction would display the same renormalization.
- [60] N. Parragh, G. Sangiovanni, P. Hansmann, S. Hummel, K. Held, and A. Toschi, Effective crystal field and fermi surface topology: A comparison of  $d$ - and  $dp$ -orbital models, *Phys. Rev. B* **88**, 195116 (2013).
- [61] J. C. Budich, B. Trauzettel, and G. Sangiovanni, Fluctuation-driven topological Hund insulators, *Phys. Rev. B* **87**, 235104 (2013).
- [62] P. Werner and A. J. Millis, Doping-driven mott transition in the one-band hubbard model, *Phys. Rev. B* **75**, 085108 (2007).
- [63] S. Rachel and K. Le Hur, Topological insulators and mott physics from the hubbard interaction, *Phys. Rev. B* **82**, 075106 (2010).
- [64] A. Rüegg and G. A. Fiete, Topological order and semions in a strongly correlated quantum spin hall insulator, *Phys. Rev. Lett.* **108**, 046401 (2012).
- [65] J.-H. Zheng, B. Irsigler, L. Jiang, C. Weitenberg, and W. Hofstetter, Measuring an interaction-induced topological phase transition via the single-particle density matrix, *Phys. Rev. A* **101**, 013631 (2020).
- [66] T. Mertz, K. Zantout, and R. Valentí, Statistical analysis of the chern number in the interacting haldane-hubbard model, *Phys. Rev. B* **100**, 125111 (2019).
- [67] J. M. Pizarro, S. Adler, K. Zantout, T. Mertz, P. Barone, R. Valentí, G. Sangiovanni, and T. O. Wehling, Deconfinement of mott localized electrons into topological and spin-orbit-coupled dirac fermions, *npj Quantum Materials* **5**, 79 (2020).
- [68] C. L. Kane and E. J. Mele, Quantum spin hall effect in graphene, *Phys. Rev. Lett.* **95**, 226801 (2005).
- [69] F. D. M. Haldane, Model for a quantum hall effect without landau levels: Condensed-matter realization of the "parity anomaly", *Phys. Rev. Lett.* **61**, 2015 (1988).
- [70] C. L. Kane and E. J. Mele,  $Z_2$  topological order and the quantum spin hall effect, *Phys. Rev. Lett.* **95**, 146802 (2005).